ROYAL SOCIETY OF CHEMISTRY

PAPER

Check for updates

Oxidation of dibenzyl ether with nitric acid to benzaldehyde in continuous-flow microreactors

Xiang Li,[a] Saier Liu,[a] Minjing Shang*[a] and Yuanhai Su [iD] *[ab]

As an important chemical, benzaldehyde (BzH) can be synthesized by oxidizing dibenzyl ether (DBE) with nitric acid (HNO$_3$). This is an environmentally friendly and chlorine-free production process, but it has problems such as intense *in situ* gas generation, low space–time yield and safety issues. This study developed a safe and efficient continuous-flow synthesis method using a packed-bed microreactor. Five critical parameters including reaction residence time, glass bead particle size, temperature, oxidant concentration, and initiator dosage were systematically investigated. Under optimal conditions (*T* = 85 °C, *d* = 104.5 μm, HNO$_3$ eq. = 3 and NaNO$_2$ eq. = 0.009), the conversion of DBE and the yield of BzH reached 80.11% and 96.35% after 17.92 min. The space–time yield was twice that of capillary microreactors and 40 times that of batch reactors. The reasons for *in situ* gas production in capillary microreactors and its negative impacts were explored. A kinetic model was developed, providing significant theoretical insights and practical value for better understanding the oxidation process and optimizing the process parameters.

1. Introduction

Benzaldehyde (BzH) is the simplest and most widely used aromatic aldehyde in industry and an important chemical raw material and intermediate product in many industrial processes, such as the synthesis of fiber auxiliaries, dyes, fragrances, medicines, seasonings, plastics, and coatings. In industry, there are several methods for producing BzH, mainly including the chlorination and hydrolysis of toluene, oxidation of benzyl alcohol, direct oxidation of toluene, direct formylation of benzene, and reduction of benzoic acid. In the reported literature, different raw materials, such as benzyl alcohol, styrene and toluene, were used to synthesize BzH through different reaction pathways with different catalysts, with a selectivity as high as 99%.[1–6] However, all of these methods are highly dependent on catalytic systems, and the long reaction time up to several hours is typically needed to achieve the high conversion and selectivity.

Some researchers have attempted to use low-value dibenzyl ether (DBE) as a raw material to synthesize BzH.[7] DBE as a main by-product from the industrial production of benzyl alcohol has a large output but limited applications.[8–14] Thus, dibenzyl ether becomes an intractable waste. As a result, the study of producing BzH from DBE has considerable research value. At present, there are relatively few studies on the reaction

mechanism of generating BzH from the oxidation of DBE by nitric acid (HNO$_3$). From the existing literature, the reaction mechanism can be inferred as shown in Fig. 1. First of all, HNO$_3$ reacts with nitrous acid to produce nitrogen dioxide containing free radicals. Subsequently, nitrogen dioxide radicals attack the carbon near the ether bond in DBE, generating DBE radicals. Nitrogen dioxide radicals continue to attack this carbon until the ether bond on the other side breaks, generating BzH and benzyl nitrite. Benzyl nitrite, under the oxidation of HNO$_3$, generates BzH and nitrite. Some of the accumulated nitrous acid will continue to react with HNO$_3$ to form nitrogen dioxide radicals, while the other part will self-react to form HNO$_3$ and nitric oxide. Nitric oxide can be oxidized by excess HNO$_3$ to form nitrogen dioxide.[15–18] When the amount of HNO$_3$ is insufficient, benzyl nitrite will hydrolyze into benzyl alcohol and nitrous acid.[17] In the case of excess HNO$_3$, benzyl alcohol will react with the excess HNO$_3$ to form BzH, which can be further oxidized to form benzoic acid by the excess HNO$_3$.[17]
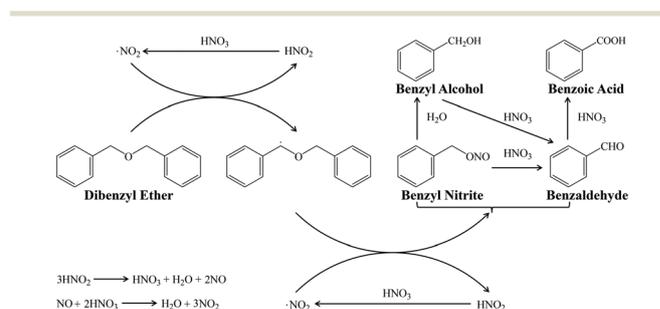
[a] *State Key Laboratory of Polyolefins and Catalysis, School of Chemistry and Chemical Engineering, Shanghai Jiao Tong University, Shanghai 200240, PR China. E-mail: mshang@sjtu.edu.cn, y.su@sjtu.edu.cn; Tel: +86 21 54738710*
[b] *Key Laboratory of Thin Film and Microfabrication (Ministry of Education), Shanghai Jiao Tong University, Shanghai 200240, PR China*

Fig. 1 Reaction mechanism of the oxidation of DBE to BzH by HNO$_3$.

At present, research on the oxidation of DBE to BzH by HNO₃ is mostly found in patents, which is often carried out in batch reactors. Since the reaction is relatively intense at high temperatures and generates a large amount of NO$_X$ gas, researchers can only adopt the dropwise feeding method to control the reaction conditions.[19] Therefore, the reaction process is limited by its mass transfer efficiency, resulting in a long reaction time and low production efficiency.

A microreactor refers to a device with a certain microstructure manufactured through precision processing technology. As a core part of microchemical technology, it can take advantage of its characteristic dimension ranging from sub-microns to sub-millimeters to achieve the purposes of increasing specific surface area, improving mixing efficiency, enhancing mass and heat transfer rates and reducing safety risks. On the one hand, by taking advantage of the large specific surface area and low resistance to heat and mass transfer, chemical reaction systems controlled by mass and heat transfer can be enhanced in microreactors.[20] On the other hand, the production processes with high safety hazards in traditional chemical industry, *e.g.*, high-temperature and high-pressure reactions,[21] peroxidation reactions,[22,23] oxidation reactions,[24] nitrification reactions,[25] sulfonation reactions,[26] hydrogenation reactions,[27] polymerization reactions,[28] *etc.*, can be improved by the use of microreactors.[29] In addition, it is convenient to explore reaction kinetics and hydromechanics,[30–32] develop various photochemical reaction paths,[33] and transform some batch processes to continuous-flow processes in microreactors.[34,35] Microreactors can be applied for multi-phase reactions, such as liquid–liquid two-phase,[36,37] gas–liquid two-phase,[38,39] and gas–liquid–liquid three-phase.[40,41]

The generation of *in situ* gas is a complex process for capillary microreactors. For instance, introducing inert gas can effectively enhance the liquid–liquid mass transfer rate,[42,43] but sometimes it may actually reduce the reaction performance.[44] However, using packed bed microreactors can effectively reduce the adverse impacts brought about by the generation of *in situ* gas.[36,45]

The research objective of this work is to regulate and optimize the rapid and highly exothermic reaction for producing BzH from DBE and HNO₃ in microreactors and to establish a low-energy consumption, efficient and safe production method. Furthermore, it aims to deeply explore the reaction mechanism and hydrodynamic characteristics, which can guide the further expanding production of BzH.

2. Experiment

2.1 Materials

Nitric acid (AR), sodium nitrite (AR), methyl orange (AR), and sodium bicarbonate (AR) were purchased from Sinopharm Chemical Reagent Co., LTD. (Shanghai, China), and dibenzyl ether (≥99%, DBE as its abbreviation) was purchased from Adamas Beta (Shanghai) Chemical Reagent Co., LTD. (Shanghai, China). *N*-Decane (≥99%) and benzyl alcohol (AR) were purchased from Shanghai Aladdin Biochemical Technology Co., LTD. (Shanghai, China), and benzaldehyde (≥99%, BzH as its

abbreviation) was purchased from Shanghai Mindray Biochemical Technology Co., LTD. (Shanghai, China). Benzoic acid (AR), *n*-hexane (AR), sodium chloride (AR), and anhydrous ethanol (AR) were purchased from Shanghai Titan Technology Co., LTD. (Shanghai, China). All reagents were used directly without further purification.

2.2 Experimental setup and procedure

The schematic diagram of experimental setup for the oxidation of DBE by HNO₃ to form BzH in a capillary microreactor or a packed-bed microreactor is shown in Fig. 2. The capillary microreactor system consisted of two micro-mixers and PFA tubes that were 1–10.5 meters long and had an inner diameter of 1 mm. The packed-bed microreactor system consisted of a micro-mixer and a 20 cm long glass tube with an inner diameter of 12 mm, in which inert glass beads (with a particle size of 104.5 μm) were filled. As a rapid reaction, there is no need to use solid catalysts instead of glass beads as the filler. Glass beads were used as filling materials to increase the surface area and promote the mixing and contact between reactants in the tube. HNO₃, DBE and sodium nitrite solutions were introduced into the microreactor system by three syringe pumps. After premixing in the micromixers, the two-phase mixture was introduced into a capillary microreactor or a packed-bed microreactor in which the oxidation reaction took place. The reaction temperature (55–85 °C) was controlled by a constant temperature water bath circulator. The residual substances were collected from the exit of the microreactor and quenched in a small bottle containing ice water. The upper organic phase was separated from the aqueous phase through a separating funnel. Each experiment was repeated three times to control the
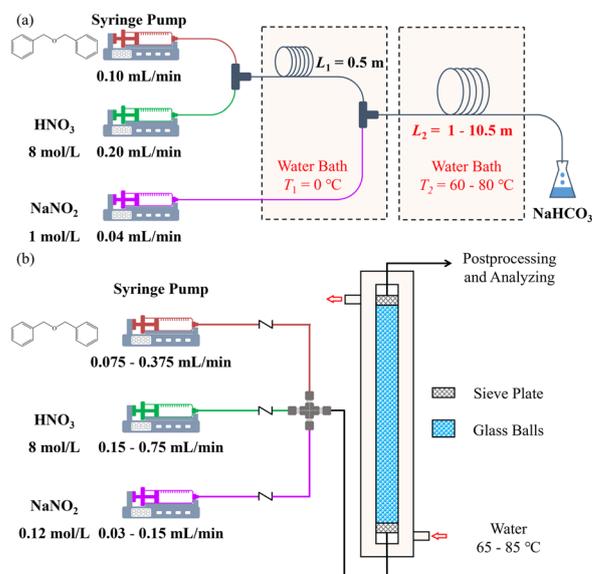

Fig. 2 Schematic representation of the capillary microreactor for the synthesis of BzH: (a) the capillary microreactor; (b) the packed-bed microreactor.

experimental error below 5%. And the average measurement value was provided as the final result.

2.3 Analysis

The concentration of HNO_3 (C_{HNO_3}) in the aqueous phase was determined by titration. Because the cost of DBE is much higher than that of HNO_3 and $NaNO_2$, it was regarded as a key component. The organic product samples mainly contained BzH, DBE and benzyl nitrite, while the contents of other polar components could be ignored. After dilution with *n*-hexane, the organic product samples were analyzed by GC (Agilent 7890B, Japan) equipped with an HP-5 column (HP-5 column, 30 m × 0.32 mm × 0.25 μm) (for details, see the SI). The conversion of DBE (X_{DBE}) is calculated by eqn (1):

$$X_{DBE} = \frac{n_{DBE}}{\dfrac{Q_{DBE} \times \rho_{DBE}}{M_{DBE}} \times t_{sample}} \tag{1}$$

where n_{DBE} represents the molar number of DBE, which is measured by the GC with the internal standard method. Q_{DBE}, ρ_{DBE} and M_{DBE} represent the volumetric flow rate, density and molecular weight of DBE, respectively. t_{sample} is the sampling time. The yield of BzH (Y_{BzH}) is calculated by eqn (2):

$$Y_{BzH} = \frac{n_{BzH}}{2 \times \dfrac{Q_{DBE} \times \rho_{DBE}}{M_{DBE}} \times t_{sample}} \tag{2}$$

where n_{BzH} represents the molar number of BzH, which is measured by the GC with the internal standard method. The selectivity of BzH (S_{BzH}) is defined by eqn (3):

$$S_{BzH} = \frac{Y_{BzH}}{X_{DBE}} \tag{3}$$

3. Results and discussion

3.1 Comparison of reaction performance in different reactors

3.1.1 Reaction within the capillary microreactor. Initially, a PFA capillary microreactor with an inner diameter of 1 mm and a length of 1–10.5 m was used for the synthesis of BzH by the oxidation of DBE with HNO_3. The experimental results are shown in Fig. 3. At a temperature of 75 °C, as the capillary length increased from 1 m to 10.5 m, the conversion of DBE increased from 13.82% to 42.16%, and the yield of BzH rose from 11.52% to 37.41%. Whether by increasing the residence time or the temperature, both the yield of BzH and the conversion of DBE would increase. However, this upward trend was gradually slowing down and did not reach the desired outcome. The results showed that in the capillary microreactor, due to the *in situ* gas production, the interfacial area of liquid–liquid two phases decreased from the initial 3.54×10^3 m^2 m^{-3} to 0.23×10^3 m^2 m^{-3}, resulting in limited reaction efficiency. For the analysis of flow patterns within capillary microreactors, please refer to the SI.

3.1.2 Comparison of reaction performance in various reactors. The oxidation performance in three kinds of reactors including the batch reactor, capillary microreactor and packed-bed microreactor are compared. As indicated in Fig. 4, when the theoretical residence time (*i.e.*, the residence time without considering the influence of the generated gas phase) was 24.25 min, the yield of BzH was no more than 40% in the capillary microreactor. The yield of BzH could reach 77.5% in the packed-bed microreactor when the residence time was extended to 33.3 min, while the yield of BzH was less than 60% with 120 min reaction time in the batch reactor. Compared with the traditional batch reactor, the characteristic channel dimension of the packed-bed microreactor is between sub-microns and sub-millimeters and much smaller. The packing glass beads providing large specific surface area were able to re-disperse continuously the biphasic reactants, and further improved the mixing efficiency and the mass transfer rate between the aqueous and organic phases, finally greatly improving the reaction efficiency. Furthermore, due to its outstanding mass transfer performance, the reactant concentration within the packed-bed microreactor is uniform, and there will be no situation of excessively high or low concentrations in certain zones as in the batch reactor, thereby avoiding the formation of by-product benzyl alcohol. According to the calculation, the space–time yield of the packed-bed microreactor was approximately twice that of the capillary microreactor and 40 times that of the batch reactor (for details, see the SI).
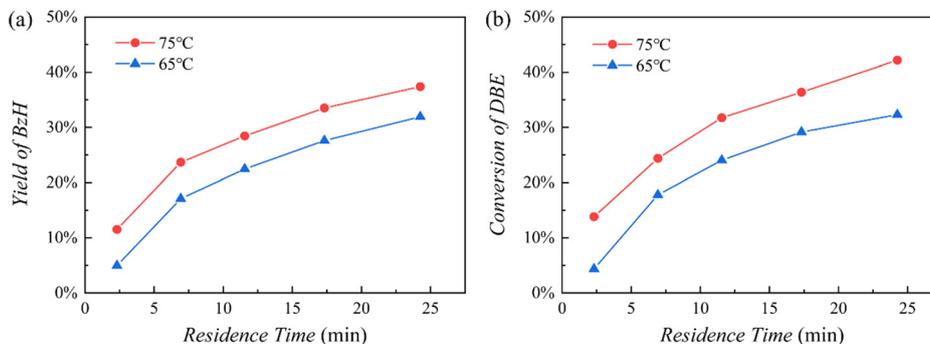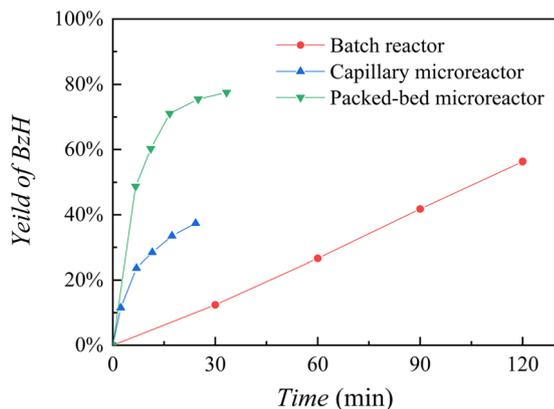

Fig. 3 (a) Effect of the reaction temperature and residence time on the yield of BzH; (b) effect of temperature and residence time on the conversion of DBE. HNO_3 eq. = 3 and $NaNO_2$ eq. = 0.076, C_{HNO_3} = 8 mol L^{-1}.

Fig. 4 Comparison between continuous-flow microreactors and batch reactor. Reaction conditions: (1) batch reactor: T = 70 °C, HNO$_3$ eq. = 3 and NaNO$_2$ eq. = 0.076, C_{HNO_3} = 8 mol L^{-1}; (2) capillary microreactor and packed-bed microreactor: T = 75 °C, HNO$_3$ eq. = 3 and NaNO$_2$ eq. = 0.076, C_{HNO_3} = 8 mol L^{-1}.

The packed-bed microreactor can also solve the problem of reduced interfacial area due to the gas production. According to our previous work, the velocity of the generated gas in packed-bed microreactors is much higher than that of the liquid.[36] It is beneficial for avoiding the effect of the *in situ* produced gas phase to the reactions to some certain extent. When the residence time was 24 min, the yield of BzH in the packed-bed microreactor was 75.47%, approximately twice that of the capillary microreactor. In contrast to the batch reactor, no by-product benzyl alcohol was produced in the packed-bed microreactor, and the reaction time was considerably reduced. In the packed-bed microreactor, the conversion of BzH could reach 60.24% in just 11.1 min, while in the batch reactor, it took more than 120 min to achieve the same level. Furthermore, the packed-bed microreactor has lower liquid holdup, and thus the oxidation process can be conducted at a higher reaction temperature with ensured safety.

3.2 Reaction condition dependence in packed-bed microreactors

3.2.1 Effect of glass bead size. The effect of glass bead size on the yield of BzH and the conversion of DBE at different

residence time was demonstrated in Fig. 5. Three different sizes of glass beads, namely 104.5 μm, 167.9 μm and 380.2 μm in average (for details, see the SI), were applied to fill the packed-bed microreactor, and the volumes of the interstices are shown in Table 1. It can be seen from Fig. 5 that both the yield of BzH and the conversion of DBE slightly increase with the decrease of the sizes of the glass beads when the residence time was kept constant. This indicated that the size of glass beads has a negligible effect on the reaction performance for the applied size range of the glass beads. The residence time distribution curve of the reactor was measured by the step tracer method (as shown in Fig. S10), and finally Bodenstedt number (Bo) was calculated to be 170.38 (for details, see the SI). According to the literature, when Bo ≥ 100, the axial diffusion of the fluid in the reactor can be ignored, indicating that the back mixing in the reactor is relatively small and can be approximately regarded as a plug flow.[46] For the consecutive reaction, plug-flow reactors can better control the reaction process. It was clear in Fig. 5(a) and (b) that both the yield of BzH and the conversion of DBE increased with increasing the residence time. When the residence time was 31.62 minutes, the yield of BzH could reach 78.33%, and the conversion rate of DBE could reach 92.48%. Moreover, the increasing trend of the yield of BzH gradually slowed down, and the selectivity of BzH increased and then decreased (Fig. 5(c)), reaching a maximum of 90.35%. This was because the produced BzH could be overoxidized to benzoic acid with the reaction proceeding, and the yield of BzH will rise to a peak and then start to decline.

3.2.2 Effect of temperature. Reaction temperature is of great importance for such complex oxidation reactions. As indicated in Fig. 6(a) and (b), both the yield of BzH and the conversion of dibenzyl increased significantly when increasing the reaction temperature. At the temperature of 85 °C and the residence time of 36.08 min, the yield of BzH reached the highest at 80.07%, and the conversion of DBE reached the highest at 97.18%. However, the selectivity of benzaldehyde first increased and then decreased with increasing the reaction temperature. At longer reaction times (>18.04 min), the selectivity of BzH at 65 °C exceeded that at higher reaction temperatures, with the
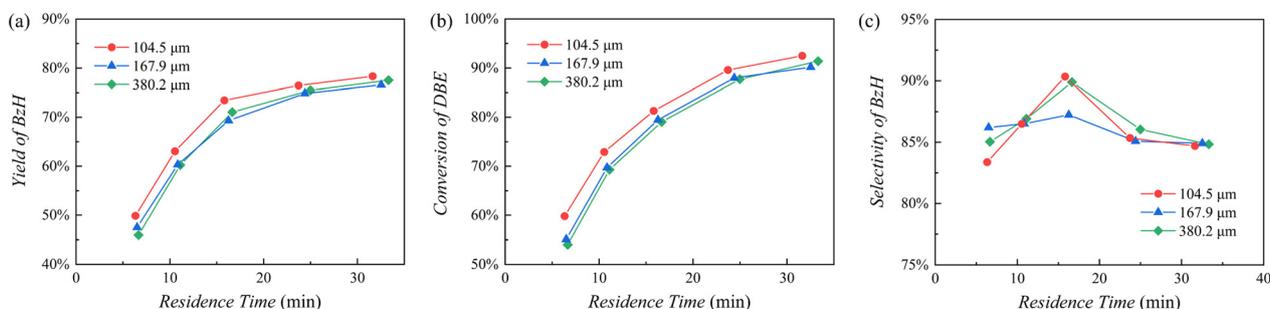
Fig. 5 (a) Effects of the particle size of glass beads and residence time on the yield of BzH; (b) effect of the particle size of glass beads and residence time on the conversion of DBE; (c) effect of the particle size of glass beads and residence time on the selectivity of BzH. T = 75 °C, HNO$_3$ eq. = 3 and NaNO$_2$ eq. = 0.076, C_{HNO_3} = 8 mol L^{-1}.

Table 1 The volumes of the interstices after filling with different sizes of glass beads

Glass bead particle size (μm)	Reactor volume (mL)
104.5	8.06
167.9	8.29
380.2	8.49

selectivity reaching up to 90.59%. The variation trend of the BzH selectivity with the reaction temperature was attributed to the overoxidation of BzH to benzoic acid, which is easier to occur at higher reaction temperatures. At the initial reaction stage, it was beneficial for the formation of BzH when the reaction temperature was higher. Higher temperature not only can promote the synthesis of BzH, but also accelerate the overoxidation of BzH. Therefore, the produced BzH was overoxidized faster at a higher temperature. As could be seen from Fig. 6(c), with the increase of the residence time at a constant reaction temperature, the selectivity of BzH first increased and then decreased.
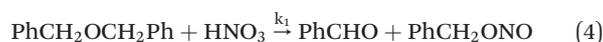
3.2.3 Effect of HNO$_3$. The influence of the concentration of HNO$_3$ as an oxidant on the reaction performance was also investigated. From Fig. 7(a) and (b), it can be seen that both the conversion of DBE and the yield of BzH increased with the increase of the HNO$_3$ concentration when the residence time was less than 20 min. When the residence time was 17.91 min, the yield of BzH reached the highest at 80.11%, and the conversion rate of DBE reached the highest at 96.35%. With extending the residence time to be longer than 20 min, the yield of BzH started to slightly decrease with at higher HNO$_3$ concentrations. A higher HNO$_3$ concentration was conducive to the conversion of DBE. However, the higher HNO$_3$ concentration not only promoted the synthesis of BzH but also accelerated its overoxidation. As a result, the yield of BzH first increased and then decreased at higher HNO$_3$ concentrations with the residence time increase. When the HNO$_3$ concentration is 10 mol L^{-1} and the residence time exceeds 25 minutes, the outlet of the packed-bed microreactor will be clogged by a large amount of benzoic acid crystals that precipitate due to cooling. From Fig. 7(c), it can be seen that the selectivity of BzH with the HNO$_3$ concentration of 6 mol L^{-1} exceeded those with higher

concentrations of HNO$_3$ at the same residence time. The selectivity at this point is the highest, reaching 88.89%. This phenomenon was attributed to the overoxidation of BzH to benzoic acid, which is more likely to occur at higher HNO$_3$ concentrations.

3.2.4 Effect of sodium nitrite. Since the reaction between HNO$_3$ and DBE to produce BzH hardly occurs in the absence of the initiator sodium nitrite, it is necessary to study the effect of sodium nitrite dosage on the reaction performance. The influence of sodium nitrite dosage on the reaction performance is depicted in Fig. 8. It can be observed that the conversion of DBE ranges from 80.36% to 81.73%, and the yield of BzH ranges from 70.36% to 73.64%, both of which remain almost constant as the molar ratio of sodium nitrite to DBE increased. This indicates that the dosage of the initiator had an almost negligible influence on the reaction outcome. From the perspective of the reaction mechanism, the necessity of the initiator lies in the first step of the reaction, that is, nitrogen dioxide radicals are generated from the reaction between HNO$_3$ and nitrous acid. Next, the generated nitrogen dioxide radicals attack DBE and then they are reduced to nitrous acid. And HNO$_3$ will also be reduced to nitrous acid after oxidizing benzyl nitrite. Overall, as long as a small amount of nitrous acid exists in the reaction system at the initial stage of the reaction process, nitrous acid can be continuously supplied.

3.3 Kinetic study on the synthesis of BzH from DBE and HNO$_3$

Based on the obtained experimental results and the mechanism shown in Fig. 1, a kinetic model of the oxidation reaction between HNO$_3$ and DBE was established. The reaction network is as shown in eqn (4) and (5).

$$PhCH_2OCH_2Ph + HNO_3 \xrightarrow{k_1} PhCHO + PhCH_2ONO \quad (4)$$

$$PhCH_2ONO + HNO_3 \xrightarrow{k_2} PhCHO + 2HNO_2 \quad (5)$$

Some assumptions are made for the reaction kinetics establishment as follows: (a) the gas–liquid–liquid three-phase can be simplified to the liquid–liquid two-phase since
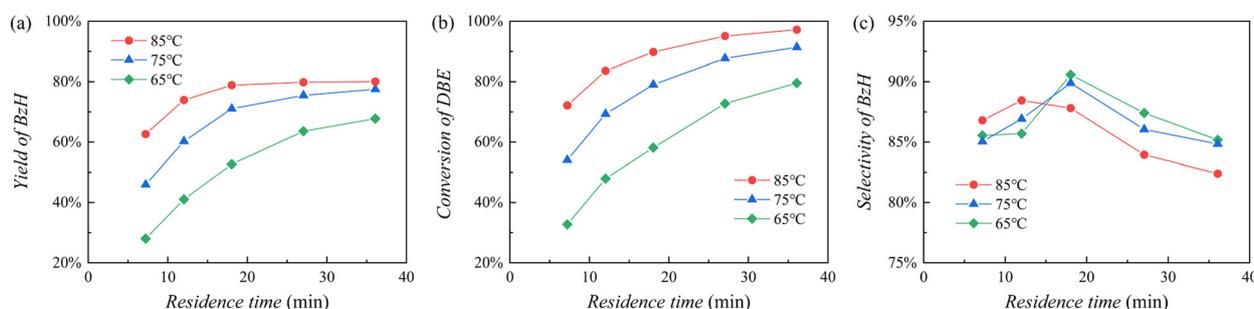
Fig. 6 (a) Effect of the reaction temperature and residence time on the yield of BzH; (b) effect of temperature and residence time on the conversion of DBE; (c) effect of temperature and residence time on the selectivity of BzH. d = 380.2 μm, HNO$_3$ eq. = 3 and NaNO$_2$ eq. = 0.076, C_{HNO_3} = 8 mol L^{-1}.

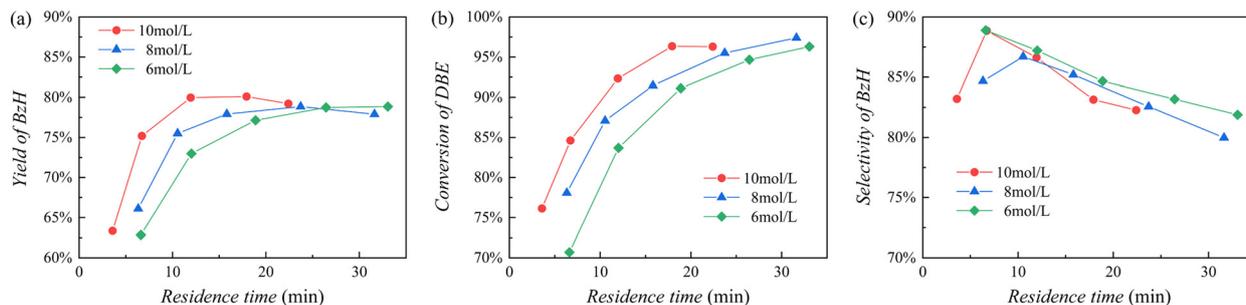**Fig. 7** (a) Effect of HNO$_3$ concentration and residence time on the yield of BzH; (b) effect of HNO$_3$ concentration and residence time on the conversion of DBE; (c) effect of HNO$_3$ concentration and residence time on the selectivity of BzH. T = 85 °C, d = 104.5 µm, HNO$_3$ eq. = 3 and NaNO$_2$ eq. = 0.009.

the velocity of the gas phase produced in the packed-bed microreactor is much higher than that of the liquid phase. (b) Due to the fact that the yields of benzoic acid and benzyl alcohol in the packed-bed microreactor were less than 5%, the further oxidation of BzH is ignored.

Therefore, the simplified reaction kinetics of the formation of BzH from DBE oxidized by HNO$_3$ can be expressed as eqn (6)–(10), which is fitted using the least squares fitting function in Python:

$$r_1 = k_1 C_{HNO_3}^a C_{DBE}^b \tag{6}$$

$$r_2 = k_2 C_{HNO_3}^c C_{BnONO}^d \tag{7}$$

$$\frac{dC_{DBE}}{dt} = -k_1 C_{HNO_3}^a C_{DBE}^b \tag{8}$$

$$\frac{dC_{BzH}}{dt} = k_1 C_{HNO_3}^a C_{DBE}^b + k_2 C_{HNO_3}^c C_{BnONO}^d \tag{9}$$

$$\frac{dC_{BnONO}}{dt} = k_1 C_{HNO_3}^a C_{DBE}^b - k_2 C_{HNO_3}^c C_{BnONO}^d \tag{10}$$

where C_{HNO_3}, C_{DBE}, C_{BzH} and C_{BnONO} are the concentrations of HNO$_3$, DBE, BzH and benzyl nitrite, respectively. k_1 and k_2 is the reaction rate constant of the oxidation reaction.
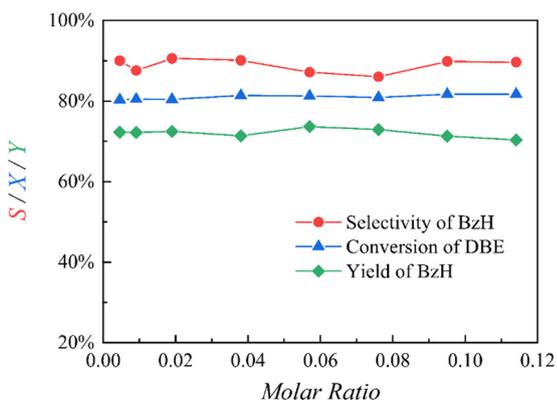

Fig. 8 Effects of the molar ratio of sodium nitrite to DBE on the reaction performance. T = 85 °C, d = 104.5 µm, HNO$_3$ eq. = 3, C_{HNO_3} = 8 mol L^{-1}.

The rate constants and reaction orders of various reactants can be fitted based on the experimental data. After obtaining the reaction rate constants at different temperatures, the relationship between ln(k) and $1/T$ was correlated, as shown in Fig. 9(a) and (b). According to Arrhenius equation, the activation energy (Ea$_1$) for the oxidation of DBE to BzH and benzyl nitrite could be determined to be 85.54 kJ mol^{-1}, and the activation energy (Ea$_2$) for the oxidation of benzyl nitrite to BzH could be determined to be 15.64 kJ mol^{-1}. The results in Fig. 10 indicate that the calculated conversion of DBE fitted well with the experimental data. Finally, the complete reaction kinetics can be established as the eqn (11) and (12):

$$\begin{aligned} r_1 &= A_1 \exp\left(-\frac{Ea_1}{RT}\right) C_{HNO_3}^{2.8} C_{DBE}^{0.7} \\ &= 1.64 \times 10^{10} \times \exp\left(-\frac{85.54 \times 10^3}{RT}\right) C_{HNO_3}^{2.8} C_{DBE}^{0.7} \end{aligned} \tag{11}$$

$$\begin{aligned} r_2 &= A_2 \exp\left(-\frac{Ea_2}{RT}\right) C_{HNO_3}^{3.4} C_{BnONO}^1 \\ &= 5.06 \times 10^{-1} \times \exp\left(-\frac{15.64 \times 10^3}{RT}\right) C_{HNO_3}^{3.4} C_{BnONO}^1 \end{aligned} \tag{12}$$

The Ha number was calculated using eqn (13) with the kinetic expressions established in the previous text (for details, see the SI) and is shown in Fig. 11, indicating that the mass transfer effect has been eliminated.[47]

$$Ha = \frac{\sqrt{\frac{2}{m+1} k C_1^{m-1} C_2^n D_{12}}}{k_L} \tag{13}$$

As shown in Fig. 12(a) and (b), the concentration of BzH and the DBE at different reaction temperatures and residence time for most of the cases involved in this work, especially at the intermediate, the predicted values of the reaction kinetics model fit well with the experimental results. However, when the reaction temperature rose to 328.15 K some of the calculated concentrations based on the kinetic model have certain errors compared with the experimental data. Especially when the residence time was 8.7 minutes, the
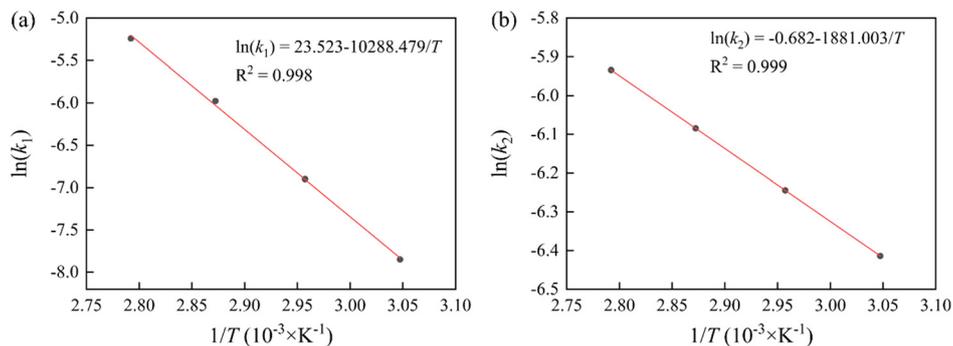
(a) $\ln(k_1) = 23.523 - 10288.479/T$
$R^2 = 0.998$

(b) $\ln(k_2) = -0.682 - 1881.003/T$
$R^2 = 0.999$

Fig. 9 Correlations between the rate constant and the temperature: (a) k_1; (b) k_2.

predicted value did not fit well with the experimental value. This is because the model does not take into account the further oxidation reaction of BzH. When the temperature is high, HNO_3 will further oxidize BzH to benzoic acid. In addition, the reactions among HNO_3, HNO_2 and NO_X will also become more complex.

4. Conclusions

Here, we report the efficient and safe synthesis of BzH from DBE with HNO_3 in microreactors for the first time. The reaction performance in the capillary microreactor, packed-bed microreactor and batch reactor was compared. The results showed that in the capillary microreactor, due to the *in situ* gas production, the interfacial area of liquid–liquid two phases decreased from the initial 3.54×10^3 m^2 m^{-3} to 0.23×10^3 m^2 m^{-3}, resulting in limited reaction efficiency. In contrast, the packed-bed microreactor, by enhancing mass transfer and rapid gas discharge, achieved a BzH yield of 60.24% at a residence time of 11.1 min. This significantly reduced the reaction time compared to the batch reactor (which required more than 120 min), and no by-product (benzyl alcohol) was produced. According to the calculation,

the space–time yield of the packed-bed microreactor was approximately twice that of the capillary microreactor and 40 times that of the batch reactor.

By calculating the residence time distribution in the packed-bed microreactor, Bo number was obtained to be 170.38. The back mixing was relatively low and the flow in the packed-bed microreactor could be approximately regarded as a plug flow, which was suitable for consecutive reactions. Five parameters including the residence time, glass bead particle size, temperature, oxidant concentration and initiator dosage were investigated. It was confirmed that increasing the residence time, temperature and oxidant concentration was conducive to improving the conversion of DBE, up to 97% at most. And the yield of BzH first went up and then slowed down and the maximum could reach up to 80%. The increase in the temperature and oxidant concentration could effectively reduce the residence time. The glass bead particle size and initiator dosage had a relatively weak influence on the conversion of DBE and the yield of BzH. Under the optimal reaction conditions ($T = 85$ °C, $d = 104.5$ μm, HNO_3 eq. = 3 and $NaNO_2$ eq. = 0.009), the conversion rate of DBE and the yield of BzH reached 80.11% and 96.35% respectively at a residence time of 17.92 min.

A simplified reaction kinetics model was established. The first step reaction of HNO_3 and DBE has a reaction order of 2.8 and 0.7, with an activation energy of 85.54 kJ mol^{-1}; the
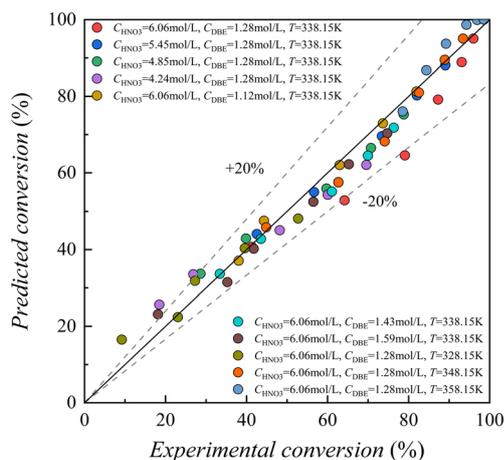

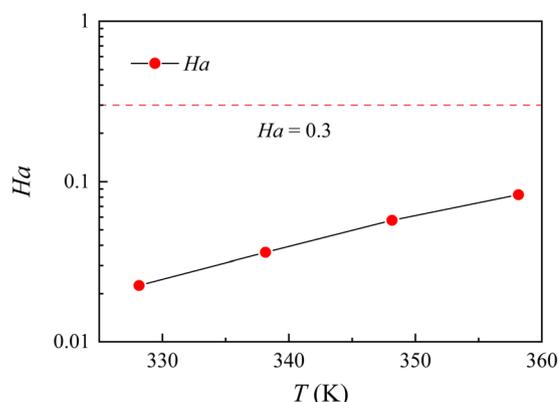**Fig. 10** Comparison between the experimental and predicted conversion of DBE.

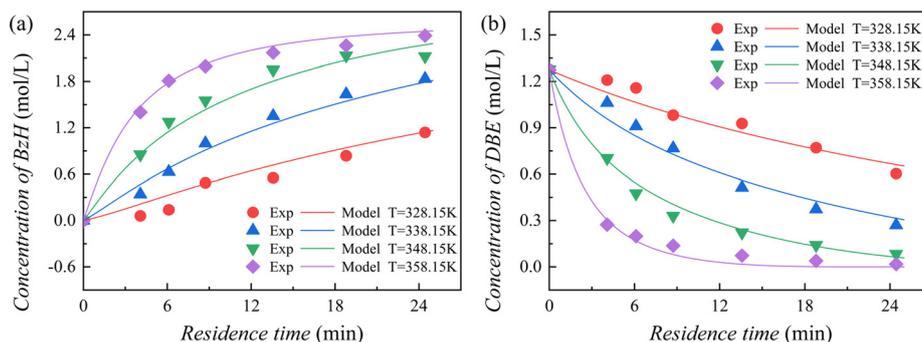**Fig. 11** Ha numbers at different temperatures.

Fig. 12 Comparison between the experimental and predicted values of the concentrations of reactants and products at different temperatures by the reaction kinetic model: (a) BzH; (b) DBE.

second step reaction of HNO_3 and benzenesulfonic anhydride has a reaction order of 3.4 and 1, with an activation energy of 15.64 kJ mol^{-1}. The predicted concentration values of the model were in good agreement with the experimental data, indicating that this model can guide the optimization and scale-up study of the continuous-flow synthesis of BzH from DBE and HNO_3.

Author contributions

Xiang Li: writing – original draft, investigation, writing –review & editing, and methodology; Saier Liu: writing –review & editing and investigation; Yuanhai Su: writing – review& editing, funding acquisition, supervision, and conceptualization; Minjing Shang: writing – review & editing and supervision.

Conflicts of interest

There are no conflicts to declare.

Data availability

The data underlying this article will be shared on reasonable request to the corresponding author.

Supplementary information (SI) is available. See DOI: https://doi.org/10.1039/d6re00004e.

Acknowledgements

References

1 X. L. Bao, H. L. Li, Z. Y. Wang, F. X. Tong, M. Liu, Z. K. Zheng, P. Wang, H. F. Cheng, Y. Y. Liu, Y. Dai, Y. C. Fan, Z. Y. Li and B. B. Huang, *Appl. Catal., B*, 2021, **286**, 119885.

2 C. Cheng, B. C. Zhu, B. Cheng, W. Macyk, L. X. Wang and J. G. Yu, *ACS Catal.*, 2023, **13**, 459–468.

3 X. H. Ren, Y. B. Wang, J. Li, K. F. Wang, M. Y. Shi, J. M. Li, J. D. Wang and C. Y. Guo, *Appl. Surf. Sci.*, 2025, **705**, 163434.

4 Y. X. Tan, Z. M. Chai, B. H. Wang, S. Tian, X. X. Deng, Z. J. Bai, L. Chen, S. Shen, J. K. Guo, M. Q. Cai, C. T. Au and S. F. Yin, *ACS Catal.*, 2021, **11**, 2492–2503.

5 M. Tayyab, Y. J. Liu, S. X. Min, R. M. Irfan, Q. H. Zhu, L. Zhou, J. Y. Lei and J. L. Zhang, *Chin. J. Catal.*, 2022, **43**, 1165–1175.

6 B. Xing, T. Wang, Z. Q. Zheng, S. J. Liu, J. J. Mao, C. Li and B. X. Li, *Chem. Eng. J.*, 2023, **461**, 141871.

7 V. P. Nekhoroshkov, G. L. Kamalov and V. I. Melnik, *React. Kinet. Catal. Lett.*, 1984, **24**, 103–105.

8 Y. S. Guan, W. Zhao, C. Zhao, D. K. Wang, L. Ao, K. S. Liu, H. M. Liu, S. L. Chen, X. Fan and X. Y. Wei, *ChemistrySelect*, 2018, **3**, 11610–11615.

9 Q. S. Guo, Q. Miao, H. L. Wei, J. H. He, X. Y. Zhou, M. Liu, J. H. Xie and W. Jiang, *Ind. Eng. Chem. Res.*, 2024, **63**, 14018–14028.

10 Z. L. Jiang, S. B. Zhu, X. F. Tang, H. B. Tang, X. M. Zhu, L. Yu, L. T. Li, Y. D. Wang, H. L. Tang and X. L. Liu, *Sustainable Energy Fuels*, 2025, **9**, 2421–2432.

11 S. A. Krokhmal and T. N. Zueva, *Probl. Atom. Sci. Technol.*, 2021, 111–114.

12 Z. Y. Li, L. Ju, R. P. Bao, X. B. Lin, T. Wang and X. H. Yu, *Synlett*, 2025, **36**, 480–483.

13 M. X. Zhao, X. Y. Wei, M. Qu, J. Kong, Z. K. Li, J. Liu and Z. M. Zong, *Fuel*, 2016, **183**, 531–536.

14 Y. N. Zheng, X. L. Song, Y. X. Fu and L. G. Gao, *J. Saudi Chem. Soc.*, 2024, **28**, 101825.

15 H. Feilchenfeld, S. Manor and J. A. Epstein, *J. Chem. Soc., Dalton Trans.*, 1972, 2675–2680.

16 Y. OGATA, in *Oxidation in Organic Chemistry 5-C*, ed. W. S. Trahanovsky, Elsevier Science & Technology, United States, 1978, vol. 5, pp. 295–342.

17 P. Strazzolini and A. Runcio, *Eur. J. Org. Chem.*, 2003, **2003**, 526–536.

18 Z. F. Yan, G. Lee, J. Deng and G. S. Luo, *Chem. Eng. Sci.*, 2025, **301**, 120757.

19 S. R. Joshi, S. B. Sawant and J. B. Joshi, *Org. Process Res. Dev.*, 2001, **5**, 152–157.

20 K. Wang, Y. Lu, H. Shao and G. Luo, *Ind. Eng. Chem. Res.*, 2008, **47**, 9754–9758.

21 X. H. Zhang, Z. Chen, J. Chen and J. H. Xu, *Chem. Eng. Sci.*, 2024, **288**, 119777.

22 M. Qiu, L. Xiang, M. Shang and Y. Su, *Adv. Polym. Technol.*, 2021, 2966912–2966920.

23 S. K. Xia, T. Yang, Z. Chen and J. H. Xu, *Chem. Eng. Sci.*, 2024, **290**, 119826.

24 G. Li, S. Liu, X. Dou, M. Shang, Z. Luo and Y. Su, *Ind. Eng. Chem. Res.*, 2021, **60**, 9389–9398.

25 Z. H. Wen, M. Yang, S. N. Zhao, F. Zhou and G. W. Chen, *React. Chem. Eng.*, 2018, **3**, 379–387.

26 T. M. Xie, C. F. Zeng, C. Q. Wang and L. X. Zhang, *Ind. Eng. Chem. Res.*, 2013, **52**, 3714–3722.

27 N. Joshi and A. Lawal, *Chem. Eng. Sci.*, 2012, **84**, 761–771.

28 L. Xiang, Z. Zhong, S. Liu, M. Shang, Z. Luo and Y. Su, *Ind. Eng. Chem. Res.*, 2022, **61**, 15917–15932.

29 K. Schubert, J. Brandner, M. Fichtner, G. Linder, U. Schygulla and A. Wenka, *Microscale Thermophys. Eng.*, 2001, **5**, 17–39.

30 S. Liu, G. Li, M. Shang, Z. H. Luo and Y. Su, *AIChE J.*, 2021, **67**, e17362.

31 M. Pasha, S. Liu, J. Zhang, M. Qiu and Y. Su, *Ind. Eng. Chem. Res.*, 2022, **61**, 12249–12268.

32 Z. F. Yan, J. X. Tian, C. C. Du, J. Deng and G. S. Luo, *Chin. J. Chem. Eng.*, 2022, **41**, 49–72.

33 Y. H. Su, N. Straathof, V. Hessel and T. Noël, *Chem. - Eur. J.*, 2014, **20**, 10562–10589.

34 L. Malet-Sanz and F. Susanne, *J. Med. Chem.*, 2012, **55**, 4062–4098.

35 J. Yoshida, Y. Takahashi and A. Nagaki, *Chem. Commun.*, 2013, **49**, 9896–9904.

36 Y. S. Liu, M. J. Shang, S. E. Liu, X. Xue, Z. H. Zhong, Q. Niu and Y. H. Su, *Chem. Eng. Sci.*, 2024, **299**, 120499.

37 C. Shen, Q. B. Zheng, M. J. Shang, L. Zha and Y. H. Su, *AIChE J.*, 2020, **66**, e16260.

38 N. Straathof, Y. H. Su, V. Hessel and T. Noël, *Nat. Protoc.*, 2016, **11**, 10–21.

39 J. Zhang, K. Wang, X. Lin, Y. Lu and G. Luo, *AIChE J.*, 2014, **60**, 2724–2730.

40 Y. Liu, G. Chen and J. Yue, *J. Flow Chem.*, 2020, **10**, 103–121.

41 J. W. Zhang, Z. Chen and J. H. Xu, *AIChE J.*, 2024, e18554.

42 T. F. Feng, J. Tan, W. S. Deng and Y. F. Su, *Chem. Eng. Sci.*, 2018, **177**, 270–283.

43 Y. H. Su, G. W. Chen, Y. C. Zhao and Q. Yuan, *AIChE J.*, 2009, **55**, 1948–1958.

44 A. Ufer, D. Sudhoff, A. Mescher and D. W. Agar, *Chem. Eng. J.*, 2011, **167**, 468–474.

45 Y. S. Liu, M. J. Shang, Q. Niu and Y. H. Su, *Chem. Eng. Sci.*, 2025, **317**, 121987.

46 N. M. Kashid, in *Microstructured Devices for Chemical Processing*, ed. A. Renken and L. Kiwi-Minsker, Wiley-VCH Verlag GmbH & Co. KGaA, Weinheim, 2014, vol. 8, pp. 89–128.

47 T. Noël, Y. H. Su and V. Hessel, in *Organometallic Flow Chemistry*, ed. T. Noel, Springer Group, Berlin, 2016, vol. 57, pp. 1–41.